Supporting Information

Sekhar et al. 10.1073/pnas.1611418113

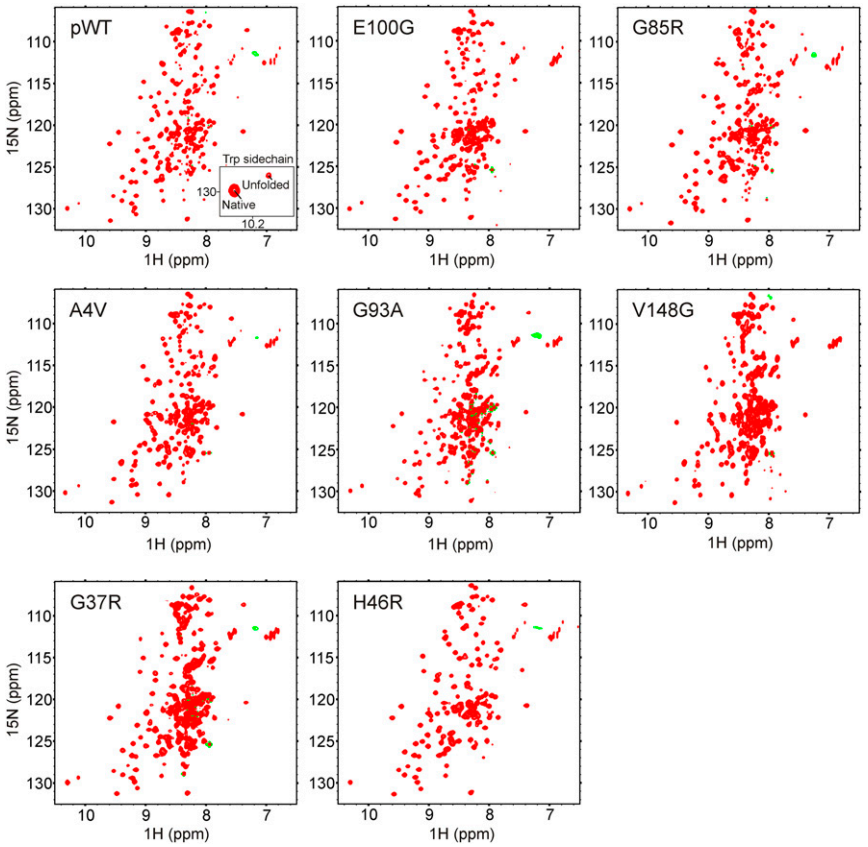

Fig. S1. ^{15}N-^{1}H TROSY-HSQC spectra of pWT and mutant proteins, 25 °C, 14.1 T. (*Inset*) Trp side-chain indole resonances of native and unfolded apoSOD1^{2SH} used for estimating $\Delta G^{0}_{unfolding}$ are shown in the spectrum of pWT.

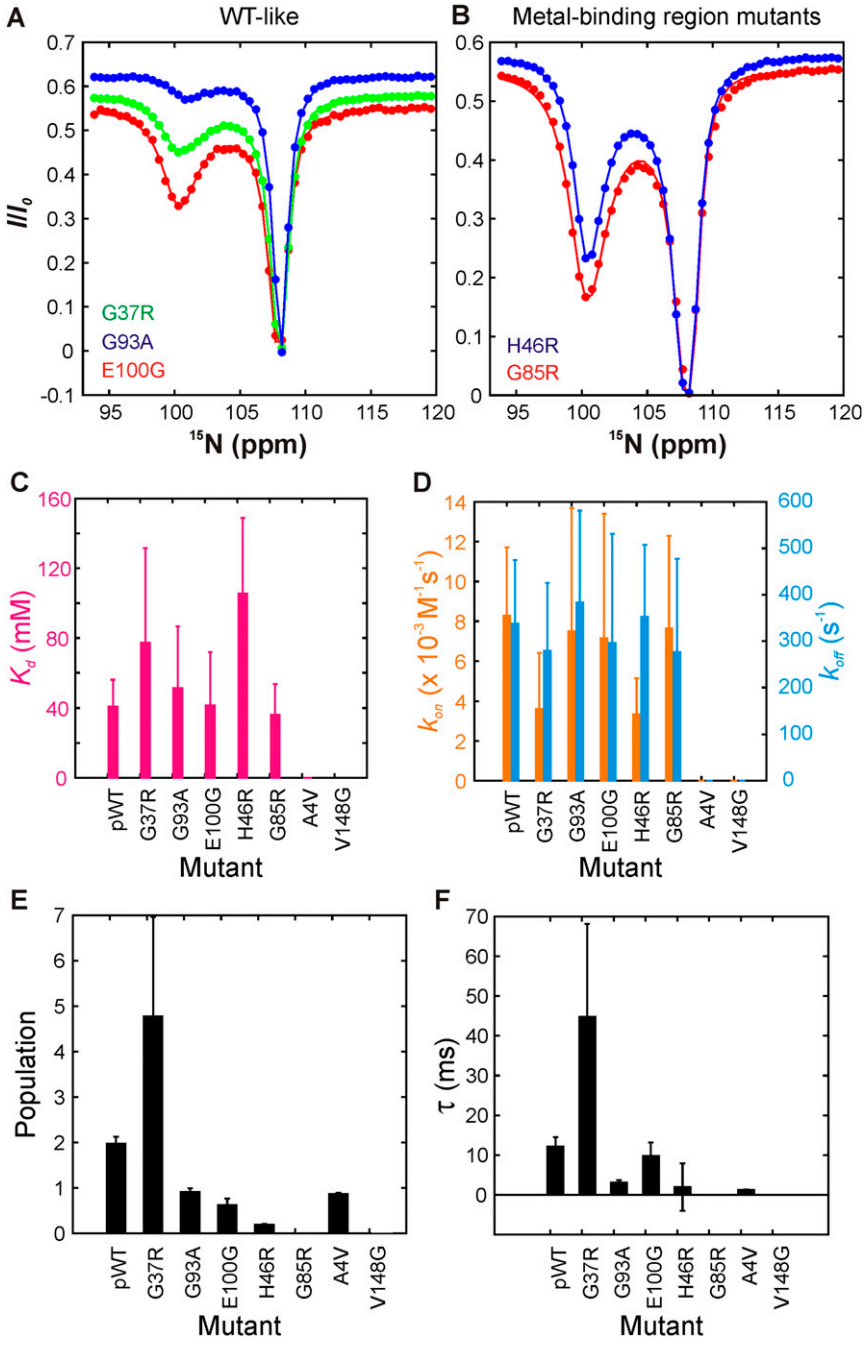

Fig. S2. ^{15}N CEST profiles for Gly-61 reporting on native dimerization (process I) for WT-like (*A*) and metal-binding region (*B*) mutants are shown. It is important to note that the sizes of the minor dips in each of the different traces cannot be compared because experiments were performed at different protein concentrations, necessitated by the fact that different mutants express at significantly different levels. For example, although G93A only shows a small minor state dip (blue in *A*), its concentration is approximately twofold and threefold smaller than for E100G and G37R, respectively, whose CEST profiles are also shown in *A*. Dissociation constants (K_d) (*C*) and association (k_{on}; orange) and dissociation (k_{off}; cyan) rate constants (*D*) for dimerization obtained by fitting residue- and B_1-specific CEST profiles to two-state models of exchange are shown, as described previously (18). Error bars correspond to 1 SD of the obtained values. The K_d, k_{on}, and k_{off} values are not listed for A4V and V148G because the dimer state could not be detected for these proteins. In this regard, it is worth noting that although a very small dip, just slightly above noise, corresponding to the dimer could be observed in CEST traces of Gly-61 of A4V (Fig. 2*C*, red), the corresponding traces for other probes at the dimer interface, including Gly-51, Asn-53, and Thr-54, did not show evidence of an excited state, at least when a B_1 field of 25 Hz was used. The lifetime and population of the excited state dimer are given by $\tau = \frac{1}{k_{off}}$ and by $p_D = \frac{2k_{on}[N]}{2k_{on}[N]+k_{off}}$, respectively, where $N = \frac{1}{4}\left(\sqrt{K_d^2 + 8K_d N_T} - K_d\right)$ and N_T is the total apoSOD1^{2SH} concentration. Excited state populations (*E*) and lifetimes (*F*) for process II (helix formation) obtained by fitting residue- and B_1-specific CEST profiles to two-state models of exchange, as described previously, are shown, with errors (1 SD of obtained values) indicated. Values are not listed for G85R and V148G because minor state dips could not be observed/quantified for these mutants.

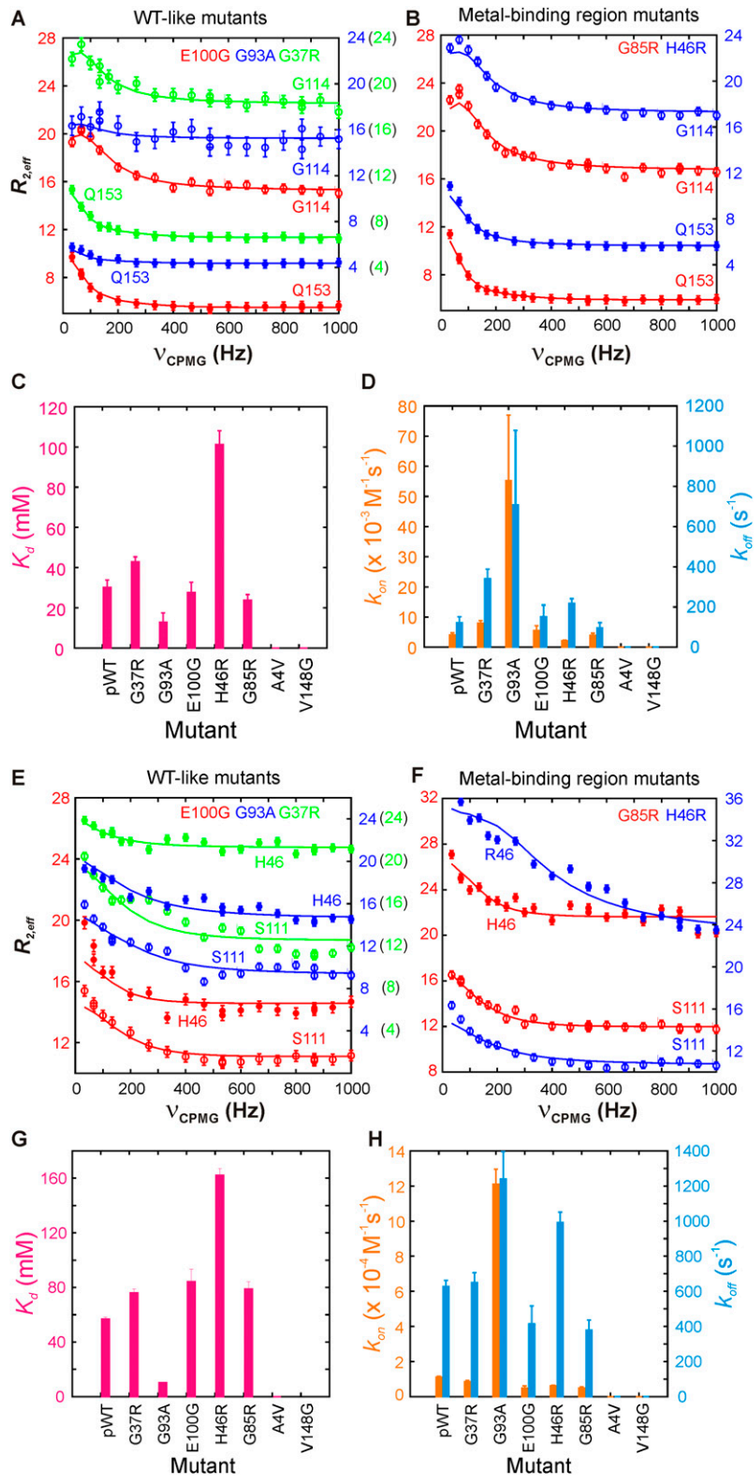

Fig. S3. ^{15}N CPMG profiles for Gly-114 (○) and Gln-153 (●), 14.1 T, reporting on process III (symmetrical nonnative dimerization) for WT-like (*A*) and metal-binding region (*B*) mutants, are shown. K_d (*C*) and k_{on} (orange) and k_{off} (cyan) rate constants (*D*) for dimerization obtained by fitting CPMG profiles to two-state models of exchange, as described previously (54), are shown. Errors in the exchange rate constants ($k_{ex} = 2k_{on}[N] + k_{off}$) and excited state populations (p_E) were obtained from the covariance matrix (55) for the fits, and uncertainties in K_d, k_{on}, and k_{off} were determined by error propagation. The lifetime of the symmetrical dimer is given by $\tau = \frac{1}{k_{off}}$, whereas its population is $p_D = \frac{2k_{on}[N]}{2k_{on}[N]+k_{off}}$, where $N = \frac{1}{4}(\sqrt{K_d^2 + 8K_dN_T} - K_d)$ and N_T is the total apoSOD1^{2SH} concentration. ^{15}N CPMG profiles of Ser-111 (○) and His-46 (●) reporting on asymmetrical nonnative dimerization (process IV) for WT-like (*E*) and metal-binding region (*F*) mutants are shown. K_d (*G*) and k_{on} (orange) and k_{off} (cyan) rate constants (*H*) for dimerization obtained by global fitting of CPMG profiles to two-state models of exchange, as described previously (54). Errors in K_d, k_{on}, and k_{off} were obtained by propagating the errors in k_{ex} (=$k_{on}[N] + k_{off}$) and p_E determined from the covariance matrix of the global fits (55). The lifetime of the asymmetrical dimer is given by $\tau = \frac{1}{k_{off}}$, and its population is given by $p_D = \frac{k_{on}[N]}{k_{on}[N]+k_{off}}$, where $N = \frac{1}{4}(\sqrt{K_d^2 + 8K_dN_T} - K_d)$ and N_T is defined as above (details are provided in ref. 54). The sizes of dispersions cannot be compared because experiments were run at different protein concentrations; however, the presence of nonflat profiles in all cases indicates that both processes III and IV can be detected for all mutants with the exception of A4V and V148G (process III and process IV very significantly reduced), and G93A (process III very significantly reduced).

Table S1. ^{15}N-^{1}H TROSY-HSQC–based folding free energy differences for apoSOD1^{2SH} variants

Variant of apoSOD1^{2SH}	$\Delta G^0_{unfolding}$, kcal/mol*
pWT†	2.2 ± 0.3
A4V	1.0
V148G	0.3
H46R	2.5
G85R	1.3
G37R	0.7
G93A	−0.2
E100G	0.5

*Values of $\Delta G^0_{unfolding}$ were calculated as $\Delta G^0_{unfolding} = RTln\frac{V_N}{V_U}$, where R is the gas constant ($R = 1.98$ cal·K^{-1}·mol^{-1}), T is the absolute temperature ($T = 298$ K), and V_N and V_U are the volumes of Trp-32 indole side-chain peaks derived from native and unfolded conformers, as measured in TROSY-HSQC spectra (23). Volumes were determined by integrating peaks using the software package Sparky (50) and were not corrected for differential relaxation of native and unfolded state magnetization during the delays in the pulse sequence.

†Error in the value for pWT was estimated as 1 SD about the mean of measurements made on three independent samples. The largest contribution to errors in $\Delta G^0_{unfolding}$ results from sample variability (extent of unfolding increases slightly over time, despite the absence of peaks reporting on degradation). Multiple samples were not available for disease mutants.